minerals

MDPI

Article

Diagenetic Evolution Sequence and Pore Evolution Characteristics: Study on Marine-Continental Transitional Facies Shale in Southeastern Sichuan Basin

Bing Zhang [1,2,3], Siyu Wen [1,2,*], Kai Yang [3], Kai Ma [4], Pengwan Wang [5], Chuan Xu [3] and Gaoquan Cao [3]

1 State Key Laboratory of Oil and Gas Reservoir Geology and Exploitation, Chengdu 610059, China; zhangb@cdut.edu.cn
2 Institute of Sedimentary Geology, Chengdu University of Technology, Chengdu 610059, China
3 College of Geophysics, Chengdu University of Technology, Chengdu 610059, China; kaiyang1992@126.com (K.Y.); alex199208@163.com (C.X.); gaoquan@stu.cdut.edu.cn (G.C.)
4 College of Energy, China University of Geosciences (Beijing), Beijing 100080, China; mk211101@163.com
5 PetroChina Hangzhou Research Institute of Geology, Hangzhou 310023, China; wangpw_hz@petrochina.com.cn
* Correspondence: wensiyu18747023@163.com

Abstract: Diagenesis and pore structure are essential factors for reservoir evaluation. marine-continental transitional facies shale is a new shale gas reservoir of concern in the Sichuan Basin. The research on its diagenesis pore evolution model has important guiding significance in its later exploration and development. However, the current research on pore structure changes, diagenesis, and the evolution of marine-continental transitional facies shale is not sufficient and systematic. In order to reveal the internal relationship between pore structure changes and diagenesis, the evolution of marine-continental transitional facies shale was tested by X-ray diffraction, field emission scanning electron microscopy, low-pressure gas adsorption, nuclear magnetic resonance, and the diagenetic evolution sequence and nanopore system evolution of Longtan Formation shale was systematically studied. The results show that the Longtan Formation shale underwent short-term shallow after sedimentation, followed by long-term deep burial. The main diagenetic mechanisms of the Longtan Formation shale include compaction, dissolution, cementation, thermal maturation of organic matter, and transformation of clay minerals, which are generally in the middle-late diagenetic stage. The pore structure undergoes significant changes with increasing maturity, with the pore volumes of both micropores and mesopores reaching their minimum values at Ro = 1.43% and subsequently increasing. The change process of a specific surface area is similar to that of pore volumes. Finally, the diagenetic pore evolution model of Longtan Formation MCFS in Southeastern Sichuan was established.

Keywords: Sichuan Basin; Longtan Formation; marine-continental transitional facies shale; quantitative characterization; diagenesis

Citation: Zhang, B.; Wen, S.; Yang, K.; Ma, K.; Wang, P.; Xu, C.; Cao, G. Diagenetic Evolution Sequence and Pore Evolution Characteristics: Study on Marine-Continental Transitional Facies Shale in Southeastern Sichuan Basin. *Minerals* **2023**, *13*, 1451. https://doi.org/10.3390/min13111451

Academic Editor: Luca Aldega

Received: 20 August 2023
Revised: 15 October 2023
Accepted: 16 October 2023
Published: 18 November 2023

1. Introduction

The study of shale gas reservoirs is currently more concerned [1–3]. In the Sichuan Basin, several organic-rich marine shale reservoirs have been discovered in recent years [4–6], providing valuable commercial industrial gas. The marine-continental transitional facies shale (MCFS) of the Longtan Formation in the Sichuan Basin has been highly concerned as the next shale gas reservoir because of its similarities in accumulation conditions and model [7–9]. Studies of shale diagenesis show that compaction, cementation, and mineral composition affect shale reservoir pores [10,11]. Shale reservoirs usually form interconnected pores systems under the interaction effects of diagenesis and the thermal evolution of organic matter (OM) [12]. In order to understand the evolution of pores in shale reservoirs, it is crucial to investigate the diagenesis of shale reservoirs [11,13]. Additionally, the study of mineral composition characteristics, diagenesis, diagenetic evolution, and pore systems

evolution of shale reservoirs is the basis of MCFS reservoir evaluation research and also the premise for revealing the accumulation model of MCFS gas. Therefore, establishing a diagenesis-pore evolution model can elucidate the impact mechanism of diagenesis on MCFS reservoirs.

Diagenetic stages of clastic rocks can be divided into syndiagenetic stages, early diagenetic stages, middle diagenetic stages, late diagenetic stages, and epidiagenetis stages (PGEPSC, 2003) [14–16]. The pore characteristics of reservoirs are different under the influence of different diagenetic evolution stages. The early diagenesis stage is dominated by compaction, and the primary intergranular pores decrease [17]. During the diagenetic stage, cementation is well developed, quartz overgrowth and iron-bearing carbonate cements are formed, pore space is destroyed by cement filling, and dissolution is also well developed [18]. In the late diagenetic stage, due to deep burial, the rock experienced compaction. Under deep burial conditions, the increase in temperature favors the thermal evolution of organic matter, leading to its thermal cracking. Therefore, strong acidic dissolution may lead to the formation of secondary pore development zones in the reservoir, providing sufficient space for oil and gas storage [19,20]. During the epigenetic stage, due to the uplift of the Earth's crust and its proximity to the surface environment, reservoirs are often subjected to the leaching of atmospheric fresh water, resulting in the generation of secondary pores, making the rocks loose and porous [21–23]. Compaction, pressolution, cementation, dissolution, metasomatism, recrystallization, etc. all belong to the category of diagenesis [24,25]. During the process of diagenetic evolution, different diagenetic processes have varying degrees of changes in the porosity and permeability space of reservoirs, resulting in different physical properties of reservoirs in different geological periods. At present, research on marine shale gas reservoirs in the Sichuan Basin is relatively mature [26–29], and research on the diagenesis and pore structure evolution of shale reservoirs mainly focuses on marine shale [30–33]. The Upper Permian Longtan Formation shale in the Sichuan Basin is a typical representative of MCFS in China, and it has a complex evolutionary process because of the organic-inorganic diagenesis, which has a significant impact on its reservoir space [12,15,34]. For the Longtan Formation shale in the Sichuan Basin, the related research still focuses on aspects of the sedimentary environment, reservoir distribution, reservoir-forming conditions, and hydrocarbon generation potential [35–38]. The research foundation related to pore structure and diagenetic evolution is relatively weak [7,39], and the comprehensive study of diagenesis and pore structure of MCFS in the Longtan Formation of the Sichuan Basin is still blank.

In this paper, X-ray diffraction (XRD), low-pressure gas adsorption (LPGA), nuclear magnetic resonance (NMR), and field emission scanning electron microscopy (FE-SEM) were used to analyze the geochemical and mineral analysis, quantitative characterization of pore structure, and qualitative characterization of pore morphology of MCFS in the Southeastern Sichuan Basin. The diagenetic evolution sequence and nanopore system evolution of MCFS in the southeastern Sichuan Basin were systematically studied, and the influence of diagenesis on MCFS reservoirs was clarified. It is a supplement to the research content of MCFS reservoirs in the Sichuan Basin and has important reference value for the exploration of marine-continental transitional shale gas in other basins in China.

2. Geological Setting

The Sichuan Basin is rich in natural gas resources and has great exploration potential [40]. The Permian Longtan Formation in the Sichuan Basin is a typical MCFS gas series [41–43]. The Dongwu movement in the late Permian made the Sichuan Basin show a very complex structural pattern. Due to the difference in tectonic framework, the sedimentary facies in different areas of the Sichuan Basin are obviously different in the same period, from river delta facies to deep water shelf facies [44,45]. Among them, the swamp-lagoon facies sedimentary environment is widely developed in the southeastern and central parts (Figure 1) [46], and a large area of coal-bearing MCFS has been deposited. The main lithology is black shale, thin siltstone, and coal seam [47]; the OM type is mainly type III [8,42].

The research well YJ1 selected in this study is located in the south-eastern region of the Sichuan Basin. The study area is characterized by a long axis anticline extending NE-SW, mainly developing NE and NW faults [48,49].

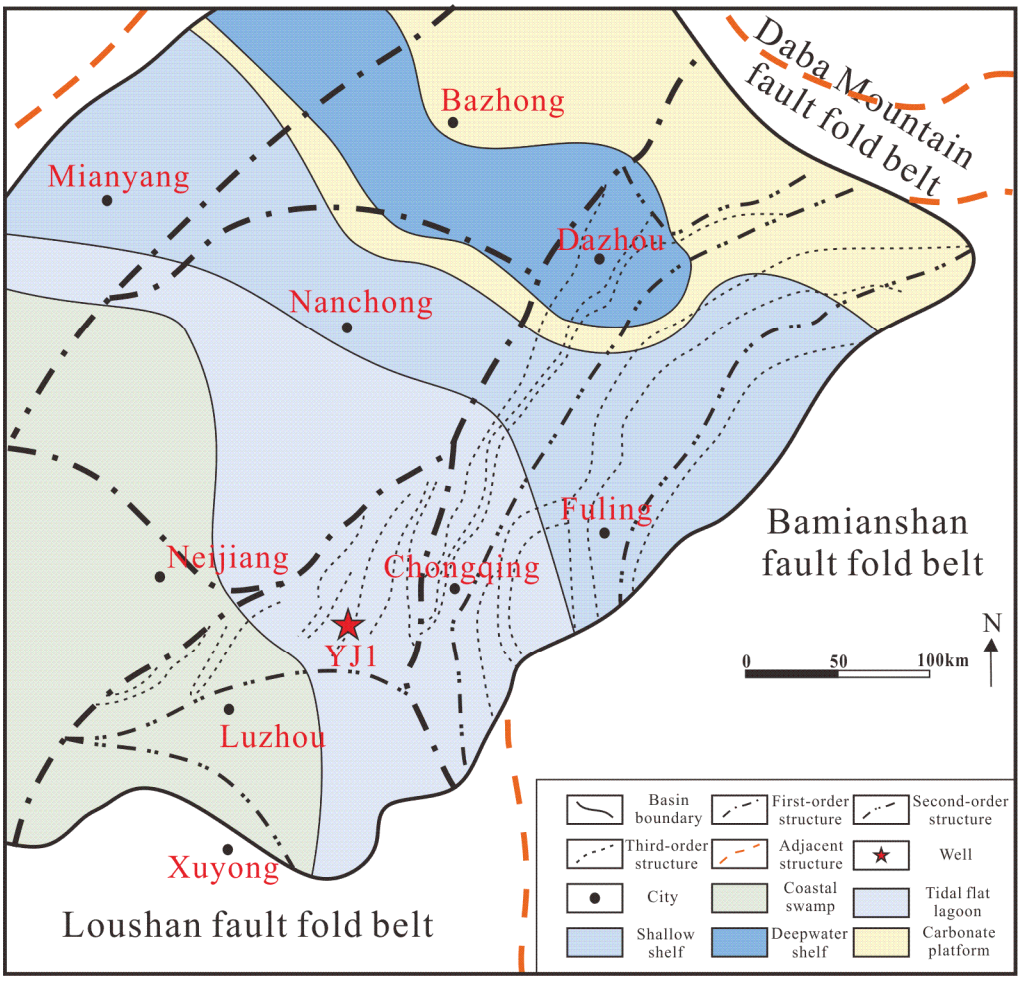

Figure 1. Sedimentary facies distribution in the Southeastern Sichuan Basin.

3. Materials and Methods

The research object of this paper is the MCFS of the third member of the Longtan Formation in the southeastern Sichuan Basin. Fresh shale samples were collected from well YJ1 (Figure 2). In order to ensure the validity of the test data, the samples are mainly taken from the fresh surface of the core sample, avoiding the calcite vein filling and other parts. The test methods adopted are mainly XRD, LPGA, NMR, and FE-SEM.

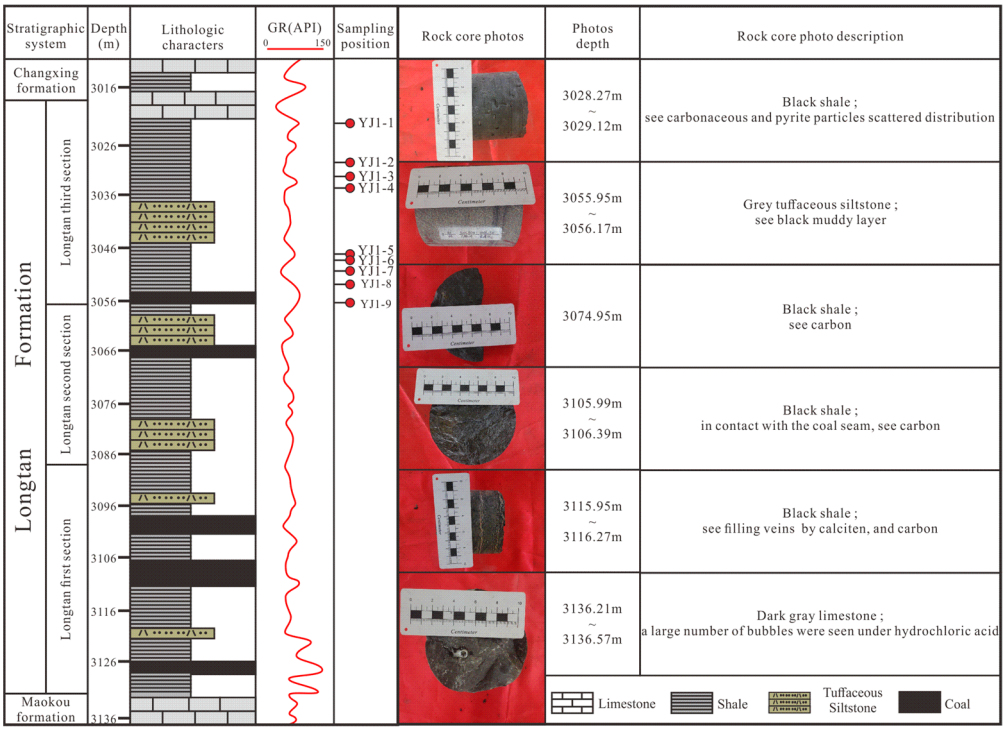

Figure 2. Comprehensive histogram of Longtan Formation MCFS, YJ1 well.

3.1. Geochemical and Mineralogical Characteristics

After HCl pretreatment to remove carbonates, the Longtan Formation samples were measured for total organic carbon (TOC) content using a LECO CS-230 analyzer, and the reflectance (Ro) of vitrinite was measured using a microscope photometer. The maximum, minimum, and average reflectance of the vitrinite were recorded. Grind all samples into a 200-mesh fine powder, and then use an AXS X-ray diffractometer (D8ADVANCE) to determine according to industry standard SY/T5163-2010 [50] at 20 °C and 70% humidity. The working voltage and current were 40 kV and 40 mA, respectively. Based on standard powder diffraction analysis data (International Data Center of the Federation), the mineral composition of shale is determined. Mineral content was calculated based on diffraction patterns and the RIR method.

3.2. Quantitative Characterization of Pore Structure

3.2.1. Low-Pressure Gas Adsorption (LPGA)

Firstly, grind and screen the shale sample to a size of 40–60 mesh. Then vacuum degassing the sample at 150 °C to remove moisture and other pollutants. Finally, perform LGPA testing on the sample. The adsorption/desorption experiments of low-pressure N_2/CO_2 gas were carried out performed at the Beijing Center for Physical and Chemical Analysis (BCPCA), which were conducted using an ASAP 2460 four-station automatic rapid specific surface area (SSA) and pore analyzer (Micromeritics, Norcross, GA, USA).

3.2.2. Nuclear Magnetic Resonance (NMR)

NMR analysis is an advanced method to analyze the pore structure and fluid distribution characteristics of shale by using NMR phenomena. Samples were saturated with water for 8 h at 25 MPa. Furthermore, NMR measurements were performed on a large sample of saturated water using an NMR analyzer to obtain the pore structure characteristics of the shale.

3.3. Qualitative Characterization of Pore Morphology

Field emission scanning electron microscopy (FE-SEM) and MAPS.

With extremely high image resolution, field emission scanning electron microscopy is effective in identifying many types of pores and their shapes in shale. Before scanning, the shale sample was processed into a 1 cm^2 scanning electron microscope thin slice. Quanta250FEG (FEI, Hillsboro, OR, USA) (working conditions: accelerating voltage: 20 kV, magnification: 50 to 300,000 times) was used to scan the samples at 24 °C and 35% humidity. Backscattered two-dimensional (2D) large-area scanning electron microscopy imaging can scan a series of continuous and overlapping high-resolution small images in a selected area for samples that require large-area observation. After the scanning is completed, these small images will be spliced to obtain an ultra-high-resolution, ultra-large-area 2D backscattered electron image.

The above two methods can provide visual evidence for the detailed observation of shale diagenesis and pore types.

4. Results

4.1. Organic Geochemical and Mineralogical Characteristics

4.1.1. Shale Composition

The samples are organic-rich shales, which have a TOC of 1.6%–4.15% (2.5% on average), and the TOC concentration increases with depth. Ro (vitrinite reflectance) content ranges from 0.56% to 3.05%, with an average of 2.16% average. The content of quartz is between 14.3% and 58% (26.5% on average). The carbonate mineral content ranges from 1.8% to 33.8% (15.2% on average), mainly composed of dolomite (0%–30%, 9.9% on average). The content of clay minerals varies between 11% and 59.6% (34.4% on average). There are other minerals (such as siderite) with a content lower than 5% that are not listed in the table (Table 1).

The quantitative characterization of clay minerals shows that the content of illite ranges from 3 to 80% (24.9% on average), the content of smectite is 0%–50% (14.7% on average), and the content of mixed layers of illite and smectite is between 13% and 56% (31.9% on average). The content of chlorite ranges from 5% to 50% (19% on average) (Table 1).

Table 1. Mineral composition and organic geochemical parameters of Longtan Formation MCFS samples, YJ1 well.

Sample ID	Depth (m)	Mineral Content (%)								Clay Mineral Content (%)								
		TOC	Ro	Quartz	Potash Feldspar	Albite	Calcite	Dolomite	Pyrite	Anatase	Manganite	Clay Mineral	S	I/S	I	K	C	I/S (S%)
YJ1-1	3021.5	1.62	0.56	14.3	2.8	5.5	20	0	22	3.4	2.9	29.1	50	28	8	9	5	19
YJ1-2	3030.95	1.6	1.43	16	5	0	7	2	10	3.6	4.4	52	34	40	10	0	16	23
YJ1-3	3031.6	3.04	2.23	21.6	2.7	8.3	2.2	14.8	4.9	4.8	6.4	34.3	19	35	6	11	29	25
YJ1-4	3034.68	2.18	2.74	26.3	0	10.3	0	12.3	6.5	7.7	4.3	32.6	0	35	4	11	50	6
YJ1-5	3050	2.41	2.61	34.2	4.2	9.1	3.8	30	6.2	0	1.5	11	0	37	14	29	20	20
YJ1-6	3050.7	2.37	1.29	22.3	8.9	0	0	1.8	0	4.5	2.9	59.6	29	56	3	4	8	22
YJ1-7	3052.55	1.81	2.51	24.4	4.2	2.6	0	14.7	1.8	8	3.5	40.8	0	13	80	2	5	22
YJ1-8	3054.77	4.15	3.05	58	0	7.6	3	7.6	0	2.2	3.2	18.4	0	20	45	12	23	5
YJ1-9	3056.8	3.32	2.98	21.1	1.7	7.4	11.4	6.6	0	9.9	10.1	31.8	0	23	54	8	15	23

4.1.2. Shale Composition

Based on the XRD test results and the current shale type classification method [51], the types of shale were classified (Figure 3). The results show that the samples taken in this study of YJ1 well in the southeastern Sichuan Basin are basically mixed shale, and there were also two samples that were clay shale.

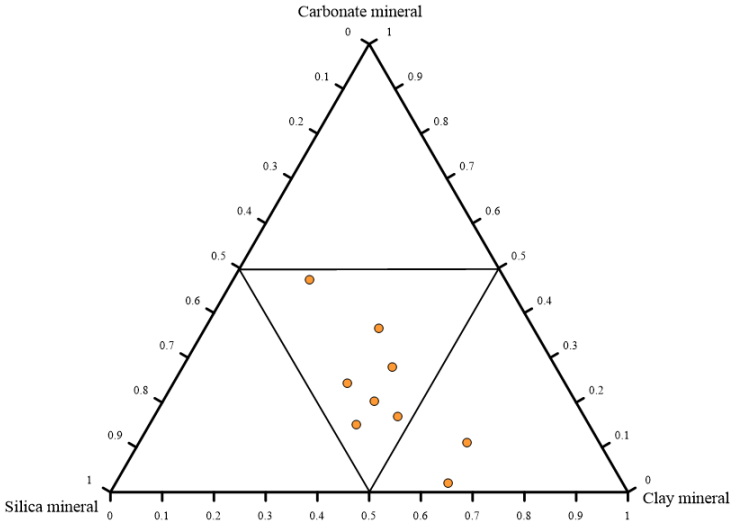

Figure 3. Division of Longtan Formation MCFS lithofacies, YJ1 well [42].

4.2. Qualitative-Quantitative Characterization of Pores

4.2.1. Qualitative Characterization of Pore Morphology

Based on the lithofacies division results of mineral components of MCFS, we use backscattered two-dimensional large-area scanning electron microscopy imaging to finely observe mixed shales and clay shales (Figure 4). Shale samples from two lithofacies contained the following three primary pore types:

1. Framework mineral pores

The framework mineral pores include intergranular pores, intragranular pores, intercrystalline pores, and dissolution pores, which are mainly developed between and inside brittle minerals. This type of pores is mainly common in mixed shale with high brittle mineral content, where dissolution pores are formed by the dissolution of soluble minerals under the action of organic acids. The dissolution pores of dolomite, calcite, and other minerals are common in mixed shale (Figure 4a,c). The intergranular pores and intragranular pores are mainly formed between or within the debris framework particles. Intergranular pores between different types of minerals can be seen in mixed shale (Figure 4c). Intercrystalline pores are typically found between various types of mineral crystals, and the intercrystalline pores of pyrite particles are the most common in mixed shale (Figure 4d).

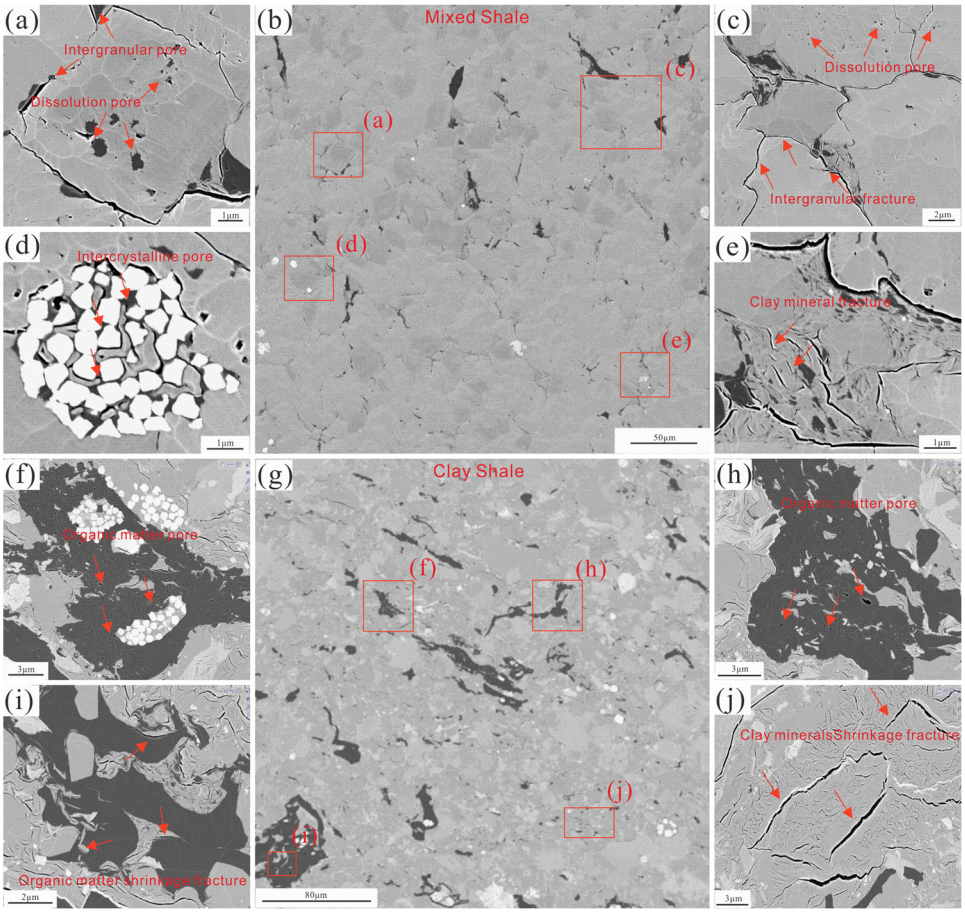

Figure 4. MAPS and FE-SEM images of different types of pores in Longtan Formation MCFS, YJ1 well. (**a**). Interanuler pore and Disslution pore; (**b**). Mixed shale, full view of Figures (a,c,d,e). (**c**). Dissolution pore and Intergranular fracture; (**d**). Intercrystalline pore; (**e**). Clay mineral fracture; (**f**). Oragnic matter pore; (**g**). Clay shale, full view of Figures (f,h,i,j); (**h**). Organic matter pore; (**i**). Organic matter shrinkage fracture; (**j**). Clay minerals Shrinkage fracture.

2. Organic matter (OM) pores

OM pores are formed by hydrocarbon generation within OM and between OM accumulations. The morphology of the pores is diverse, and various forms such as circular and serrated can be seen (Figure 4f,h). The OM pores are mainly distributed in two forms: aggregated and dispersed. The first type of OM pores is mainly developed in the whole piece of OM, which is densely distributed in a honeycomb shape and connected with each other, but with smaller pore diameters. The second type of OM pores are more scattered, have bigger diameters, and are essentially not related to one another.

3. Fracture pores

According to the observation, there are three different types of microfractures in the MCFS. The first type is fractures in skeletal minerals, usually developed within particles or at the edges of debris with good connectivity (Figure 4c). The second type is shrinkage fractures (Figure 4i), usually formed at the edges or inside of OM with a curved shape and good connectivity. The third type is the clay mineral shrinkage joint between clay minerals (Figure 4j).

4.2.2. Pore Structure and Qualitative Characterization

1. Low-pressure gas adsorption

Previous studies on shale suggest that shale pores are mainly mesopores and micropores [52–54]. The method of characterizing mesopores (2–50 nm) in shale by N_2 adsorption

and micropores (0–2 nm) by CO_2 adsorption was proposed [55,56]. Adsorption isotherms are divided into five types (types I–VI), hysteresis gyrus is divided into four types (types H1–H4), and pore fractures are divided into micropores less than 2 nm in diameter), mesopores (2 nm to 50 nm), and macropores (more than 50 nm in diameter) by the International Union of Pure and Applied Chemistry (IUPAC) [56].

The results of this study show that the hysteresis loop in the N_2 adsorption-desorption curve of MCFS is H3–H4 type (Figure 5a). The pore size distribution of mesopores is between 2–4 nm and 20–40 nm. The pore size distribution of micropores is near the two peaks of 0.55 nm and 0.85 nm. The pore volume (PV) of micropores in shale ranges from 0.00186 to 0.0296 cm^3/g (0.0023 cm^3/g on average), and that of mesopores varies between 0.0196 and 0.0296 cm^3/g (0.0253 cm^3/g on average).

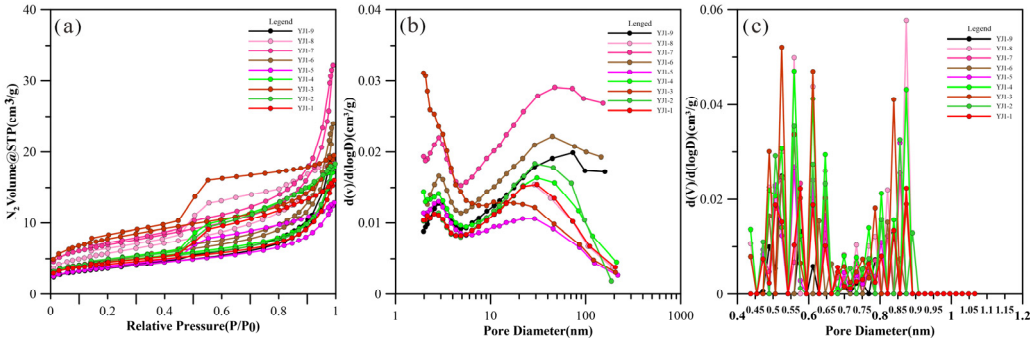

Figure 5. N_2 adsorption-desorption curve and pore size distribution characteristics of mesopores and micropores in Longtan Formation MCFS, YJ1 well. (**a**). N_2 adsorption-desorption curve; (**b**) The pore structure distribution curve of low temperature N_2 adsorption; (**c**) The pore structure distribution curve of low-temperature CO_2 adsorption.

2. Nuclear magnetic resonance

In this paper, porosity and pore structure parameters are analyzed based on the transverse relaxation time distribution of NMR [57–62]. During the testing process, it was found that there was a very high positive correlation between the porosity obtained by weighing and the porosity obtained by nuclear magnetic resonance (Figure 6). Therefore, the porosity obtained by the nuclear magnetic method can represent the porosity of the sample itself. Through nuclear magnetic resonance measurement, the porosity of the selected 9 samples ranged from 1.5% to 5.6% (3.16% on average), and the PV obtained by NMR was between 0.19 cm^3 and 0.57 cm^3 (0.36 cm^3 on average) (Table 2).

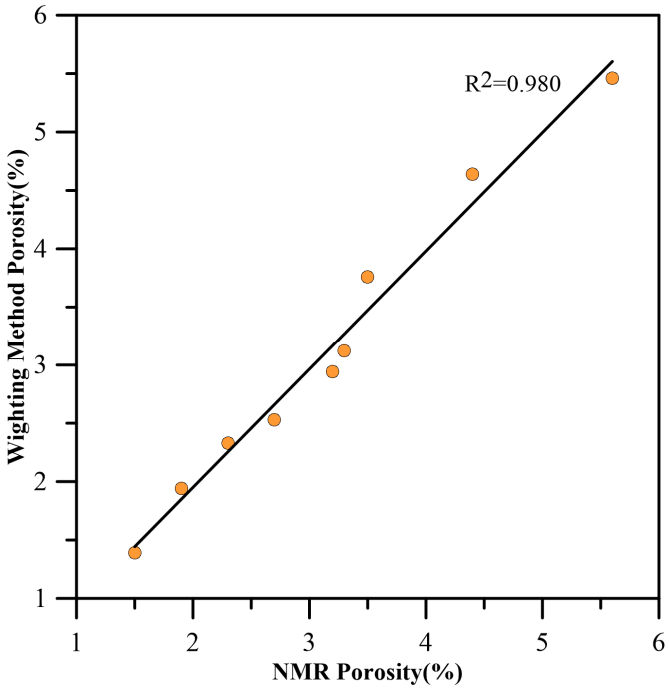

Figure 6. NMR porosity distribution characteristics of Longtan Formation MCFS samples, YJ1 well.

Table 2. Pore structure parameters of Longtan Formation MCFS samples, YJ1 well.

Sample ID	Depth (m)	Lithology	CO_2 Adsorption		N_2 Adsorption		NMR	NMR
			PVDFT (cm^3/g)	SSADFT (m^2/g)	PVBJH (cm^3/g)	SSABET (m^2/g)	PV (cm^3)	Porosity (%)
YJ1-1	3021.5	Mixed shale	0.00287	14.68	0.0226	10.48	0.25	3.2
YJ1-2	3030.95	Mixed shale	0.00186	11.43	0.0196	7.42	0.37	1.5
YJ1-3	3031.6	Mixed shale	0.00225	14.97	0.0258	8.76	0.28	2.7
YJ1-4	3034.48	Mixed shale	0.00173	16.68	0.0235	12.91	0.31	4.4
YJ1-5	3050	Mixed shale	0.0028	15.15	0.0292	12.68	0.39	3.5
YJ1-6	3050.7	Clay shale	0.00207	14.68	0.0234	7.81	0.19	2.3
YJ1-7	3052.55	Clay shale	0.00186	12.43	0.0245	11.79	0.57	1.9
YJ1-8	3054.77	Mixed shale	0.00296	19.459	0.0292	9.55	0.41	5.6
YJ1-9	3056.8	Mixed shale	0.00233	14.73	0.0296	9.31	0.43	3.3

5. Discussion

5.1. Types and Characteristics of Diagenesis

5.1.1. Compaction

Compaction is one of the most important diagenetic processes in the MCFS of the Longtan Formation. The depth of the selected well, YJ1, is greater than 3000 m. Therefore, the primary cause of the shale is the lithostatic pressure generated by the strata above it. The Longtan Formation shale was subjected to long-term subsidence after sedimentation, and the Longtan Formation shale was subjected to strong compaction. Based on the observation of FE-SEM images, it was found that clay minerals were aligned parallel to the bedding (Figure 7a), and the original kaolinite particles were fractured (Figure 7b).

5.1.2. Dissolution

The organic acids formed during the thermal evolution of OM are the main cause of shale dissolution. Organic acids can dissolve soluble minerals like calcite (Figure 7c), feldspar (Figure 7d), and dolomite (Figure 7e) to form irregularly shaped intragranular and intergranular dissolution pores. In the Longtan Formation, dissolution plays a significant

role in the formation and growth of shale reservoir spaces [63]. However, the shale in the Longtan Formation is affected by volcanic activity and contains multiple layers of volcanic ash, and an important feature of volcanic ash is that its surface acids, metal salts, and adsorbed gases are highly soluble [64]. Therefore, we speculate that the acid responsible for the dissolution of shale in the Longtan Formation may come from two sources: (1) the thermal evolution of OM; and (2) the input of volcanic material.

5.1.3. Cementation

There are siliceous, carbonate, and pyrite cement filled in the pores of the shale in the Longtan Formation. According to the formation time, it can be divided into two types. The first type is early siliceous cementation, mainly occurring in the early diagenetic stage A. The cement is authigenic microcrystalline quartz formed between pores (<20 μm). The silicon comes from the dissolution of feldspar and likely from the smectite-to-illite conversion (Figure 7f). Early carbonate cementation mainly occurred in the A stage from syndiagenesis to early diagenesis [63], and the cement materials were mainly small microcrystals of calcite and iron dolomite (Figure 7h) filled in the original pores. The second type is late siliceous cementation, mainly occurring in the middle diagenetic stage A, with the cementitious material being amorphous microcrystalline quartz, often coexisting with illite (Figure 7g). The late carbonate cementation mainly occurred in the early diagenetic stage B stage [65], with the cementation mainly composed of calcite and filling some dissolution intergranular pores (Figure 7i).

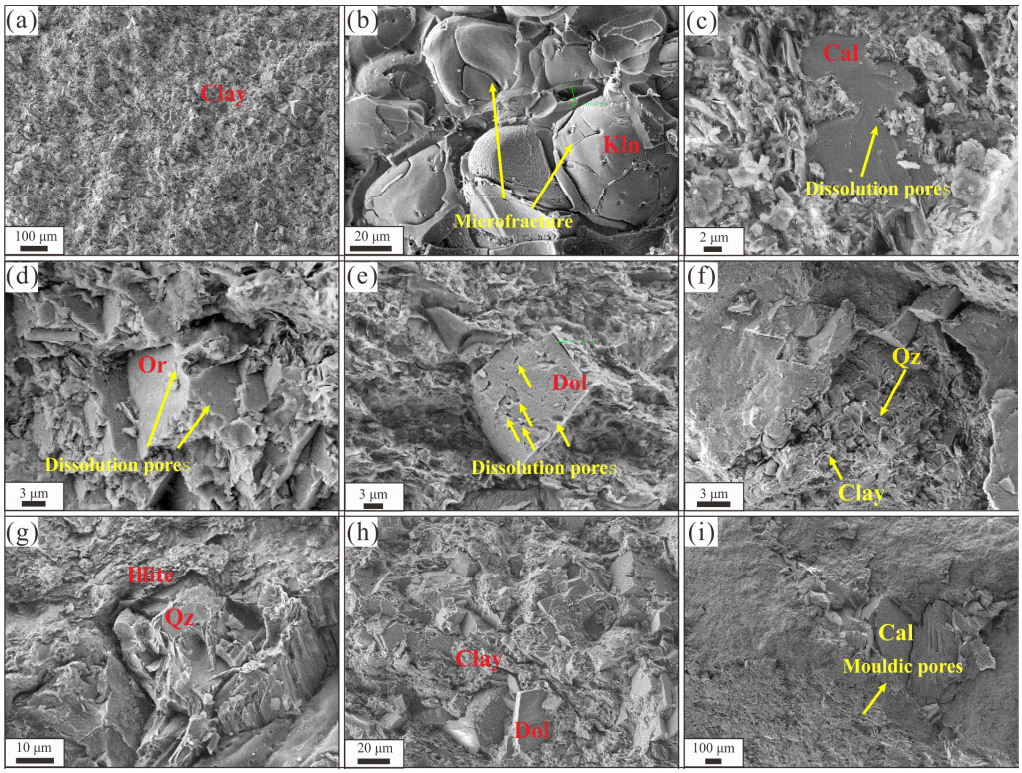

Figure 7. Characteristics of compaction, dissolution, and cementation in Longtan Formation MCFS, YJ1 well. (**a**). Compaction, clay minerals appear to be directionally distributed and have a dense structure, YJ1-1, 3021.5 m; (**b**). Compaction, microfracture appear on the surface of kaolinite particles, YJ1-1, 3021.5 m; (**c**). Dissolution, the development of dissolution pores in calcite, YJ1-6, 3050.7 m; (**d**). Dissolution, with a small amount of dissolution pores developed in granular potassium feldspar, YJ1-1, 3050.7 m; (**e**). Dissolution, the development of dissolution pores in dolomite YJ1-2, 3030.95 m; (**f**). Early siliceous cementation, the formation of authigenic microcrystalline quartz between pores, YJ1-1, 3021.5 m; (**g**). Late siliceous cementation, accompanied by amorphous microcrystalline quartz and illite, YJ1-6, 3050.7 m; (**h**). Early carbonate rock cementation, with the cementitious material being iron dolomite, YJ1-1, 3021.5 m; (**i**). Late carbonate rock cementation, with calcite as the cementitious material, YJ1-2, 3030.95 m. Kaolinite: Kln: Dolomite: Dol; Calcite: Cal; Quartz: Qz; Orthoclase: Or.

5.1.4. Clay Mineral Transformation

The clay minerals in shale transform with an increase in burial temperature. The main transformation mode of clay minerals in shale is from smectite to I/S and illite [66,67]. The organic acids generated during the thermal evolution of OM will accelerate the dissolution of potassium feldspar, promote the transformation of smectite into I/S and illite, and thereby improve the pore connectivity of the formation [68]. In the FE-SEM image, a large number of I/S in the form of flocs, filaments, and flakes can be observed, indicating a higher degree of transformation from montmorillonite to illite and I/S (Figure 8a–e). In addition, there is also kaolinite transformed from smectite in the transitional shale of the Longtan Formation, which is mostly distributed in granular form and has a relatively low content (Figure 8f).

5.1.5. Organic Matter Thermal Maturity

Longtan Formation MCFS has high TOC and Ro ranges from 0.56 to 3.05%, indicating good hydrocarbon generation potential. Under the observation of FE-SEM images, it can be found that there are pit-shaped, slit-shaped, and oval-shaped vents formed by thermal evolution in shale, and honeycomb-shaped, oval-shaped, irregular-shaped, or flaky vent groups can also be seen (Figure 8g–i). During the thermal evolution of OM, organic acids are generated, and the acidified environment promotes dissolution, forming secondary

inorganic pores [69]. Therefore, the presence of dissolution pores can also be observed around the OM (Figure 8i).

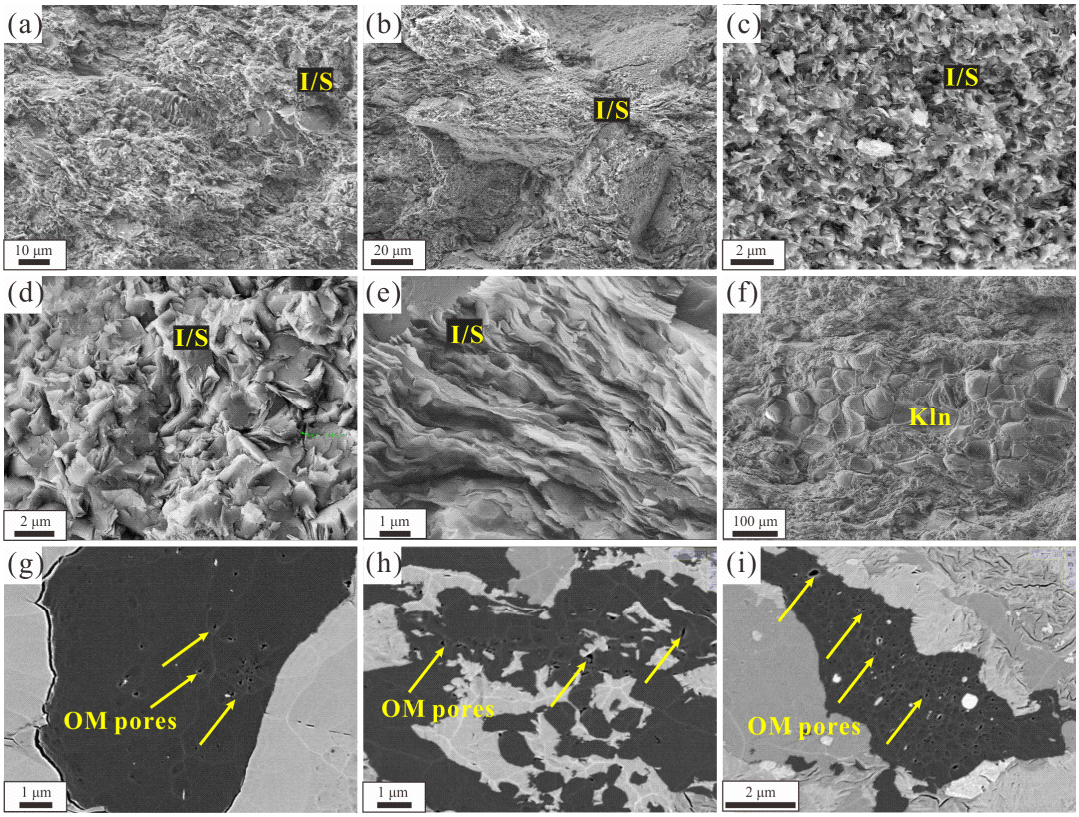

Figure 8. Characteristics of clay mineral transformation and thermal evolution of OM in MCFS, YJ1 well. (**a**,**b**). Different forms of I/S, YJ1-3, 3031.6 m; (**c**–**e**). Different forms of I/S, YJ1-4, 3034.68 m; (**f**). Kaolinite particles, YJ1-3, 3031.6 m; (**g**,**h**). Different forms of OM pores, YJ1-9, 3056.8 m; (**i**). Corrosion pore around the organic matter, YJ1-8, 3054.77 m.

5.2. Diagenetic Evolution Process

5.2.1. Diagenetic Stage

This study divides the diagenetic stages of shale in the Longtan Formation into multiple aspects, such as burial history, thermal maturity, clay mineral morphology, and porosity, relying on the Chinese oil and gas industry standard SY/T5477-2003 [14].

1. The shale porosity of the Longtan Formation varies between 1.5 and 5.6% (3.16% on average). The OM pores, clay mineral lamellar pores, and microfractures are well developed, the residual primary pores are smaller, and a small amount of dissolved pores are observed. The clay mineral lamellar pores and micro-fractures are aligned in an orientation. At low porosity, the secondary pores are mainly diagenetic pores. According to the FE-SEM images, filamentous and flaky illites and leafy chlorites can be identified. Dissolution of carbonate cement and detrital particles (e.g., feldspar) was observed in some samples, but smectite did not exist. It shows that the Longtan Formation shale has basically reached the A stage of the middle diagenetic stage.
2. In clay minerals, the content of smectite ranges between 0 and 50% (14.67% on average), I/S is 13%–56% (31.89% on average), illite ranges between 3 and 80% (24.89% on average), chlorite is 0%–29%, and kaolinite ranges from 5 to 50%. The characteristics of authigenic minerals show that smectite is widely transformed into I/S, illite, chlorite, and kaolinite. And the smectite content in the I/S ranges between 5% and 25% (22.2% on average). It shows that the Longtan Formation shale is in stage A of the middle diagenesis stage. The clay mineral assemblage is composed of mixed layers of illite-smectite + illite + chlorite and illite-smectite mixed layer + illite + chlorite + kaolinite. In addition, through the

analysis of the burial and thermal history of the Longtan Formation in the Sichuan Basin, it is found that the maximum burial depth of the Longtan Formation shale is 4000 m, and the maximum temperature reaches 140 °C–160 °C, indicating that the Longtan Formation shale is in the middle diagenetic stage B [70].

The vitrinite reflectance of the samples from the study area ranges from 0.56 to 3.05%, and the smectite content in the I/S is at least 5%. In summary, the diagenetic evolution of the Longtan Formation shale in the southeastern Sichuan Basin has reached at least the middle-late diagenetic stage (Table 2), which is consistent with previous research results on the diagenetic stage of the Upper Permian Longtan Formation shale in the surrounding areas of the Sichuan Basin [71]. The shale samples located near two layers of tuffaceous siltstone in the study interval exhibit high Ro values compared with other shale samples, which may be related to volcanic activity in the Permian. Volcanic activity can severely roast the surrounding source rocks, generating abnormally high temperatures. This accelerates the thermal evolution of hydrocarbon source rocks, rapidly reaching a high to overly mature stage, thereby improving the generation of hydrocarbons [72–74].

5.2.2. Diagenetic Evolution Sequence

Combining the diagenesis characteristics, diagenetic environment, and burial history (Figure 9), it is considered that the Longtan Formation MCFS has experienced three diagenetic evolution stages. It should be noted that the diagenetic evolution of the Longtan Formation marine continental transitional shale in the southeastern Sichuan region reached at least the middle to late diagenetic stage. However, samples from the early stages of late diagenesis cannot exclude the impact of volcanic activity. Therefore, only samples in middle diagenetic stage B and before correspond to burial histories. The three diagenetic evolution stages are as follows:

1. From the Late Permian to the Middle Triassic, the Longtan Formation MCFS experienced slow subsidence, with a burial depth of <800 m and a low formation temperature (Figure 9). Microcrystalline calcite is formed in Longtan Formation shale, and dissolution pores appear in silicate minerals such as quartz. At that time, the pores in the shale of the Longtan Formation were mainly primary mineral pores [75]. The increase in burial depth, compaction, and pressure dissolution seriously damages the shale reservoir space, leading to a significant reduction in primary pores and a clear and dense pore reduction effect on clay shale [16].
2. From the Middle Triassic to the Late Jurassic, the strata rapidly subsided and were buried deeper, beginning to generate hydrocarbons. The maximum burial depth reaches 3200~4000 m, and the maximum temperature is about 120~140 °C. The shale is rapidly consolidated (Figure 9), and the OM and kerogen begin to produce gas and acid. Numerous OM pores were created during this process. Simultaneously, plenty of organic acids cause soluble minerals (such as calcite, dolomite, feldspar, etc.) to start dissolving heavily, which favors the growth of porosity and the expansion of the matrix PV of mixed shale [76]. It was observed in the FE-SEM images that the primary intergranular pores decreased and the secondary pores increased. Smectite is converted to I/S in large quantities, and an ordered mixed-layer band is produced. At the edge of quartz, the siliceous compounds created during mineral transformation are cemented close by and create tiny secondary pores [16].
3. Since the Late Jurassic, the Longtan Formation shale has undergone a second subsidence, with a burial depth of more than 4000 m and complete consolidation of the rock (Figure 9). The primary intergranular pores essentially faded away, and the OM entered the threshold for generating gas. Clay mineral mixing layers gradually change from disordered to long-range ordered, and smectite basically disappears.

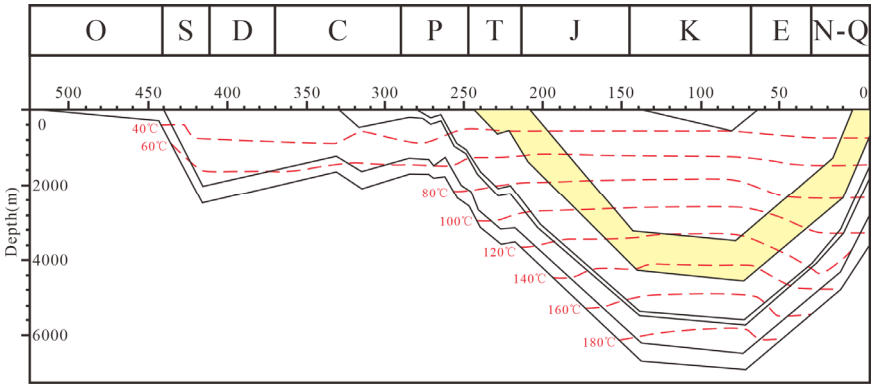

Figure 9. Burial history of Longtan Formation MCFS, YJ1 well (Modified according to [61]).

5.3. Pore Evolution

5.3.1. Relationship between Porosity and TOC, Ro, Clay Minerals

Figure 10a depicts the relationship between porosity and TOC, and there is a positive linear relationship between porosity and TOC (R^2 = 0.459). It shows that the enrichment of OM has a certain correlation with the formation of pores. At the same time, with the increase in maturity, the porosity of Longtan Formation shale decreases first and then increases, reaching its minimum value at Ro of 1.5% (Figure 10b). The decrease in porosity at Ro < 1.0% may be due to the blockage of pores and pore throats by hydrocarbons generated by OM, and the mechanical compaction at this time is also an important driving factor for the decrease in porosity. When the maturity is higher than 1.5%, the formation of plenty of organic pores and a rise in porosity in the Longtan Formation shale may be caused by the expelling of produced hydrocarbons from pores and pore throats. The soluble minerals in the Longtan Formation shale are dissolved by the acidic fluid generated at this stage, thus forming more dissolution pores.

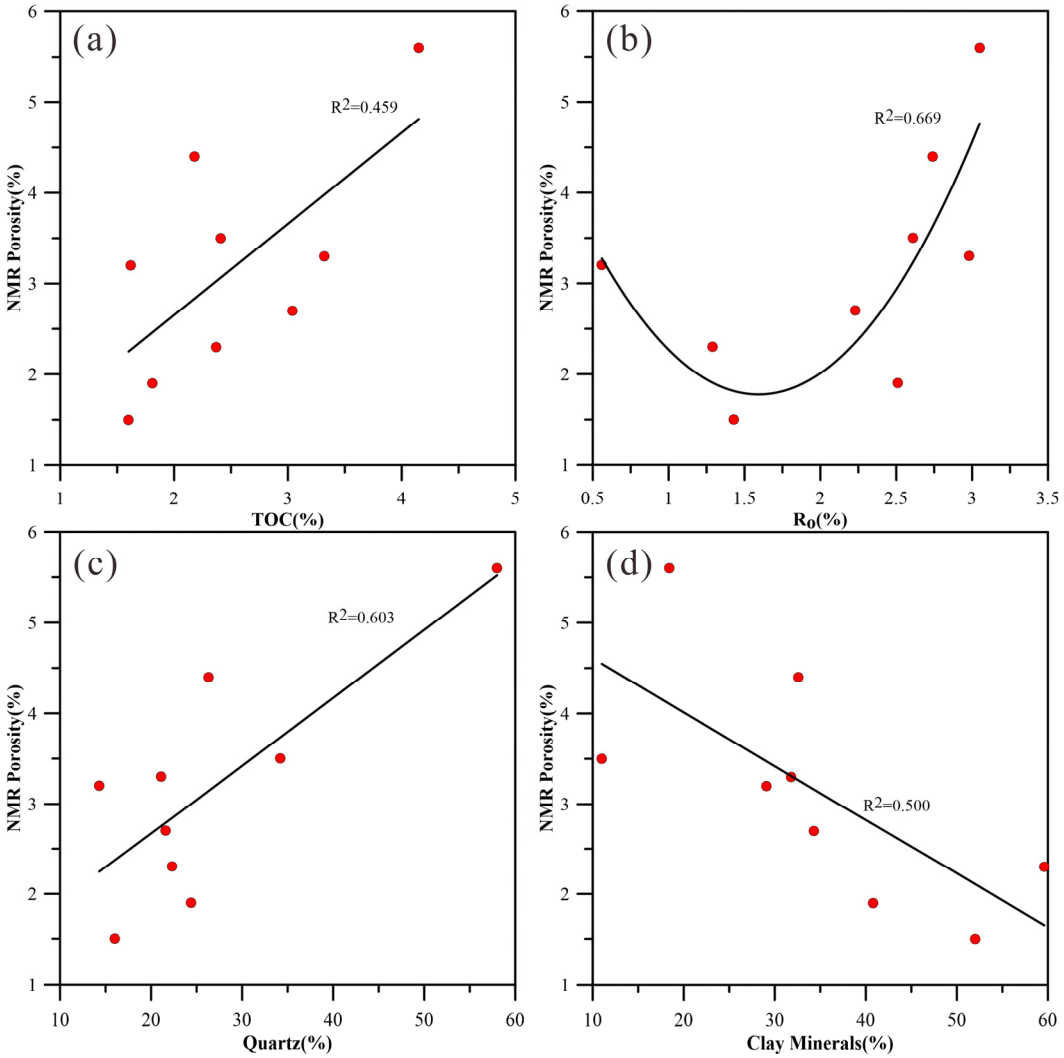

Figure 10. The relationship between porosity and TOC%, Ro and main mineral components of Longtan Formation MCFS, YJ1 well. (**a**). The Relationship between TOC and NMR Porosity; (**b**). The Relationship between Ro and NMR Porosity; (**c**). The Relationship between Quartz content and NMR Porosity; (**d**). The Relationship between Clay Minerals content and NMR Porosity.

Figure 10c,d illustrates the association between porosity and the quartz and clay mineral contents. Porosity and quartz content have a positive linear relationship (Figure 10c, R^2 = 0.603). This is because the rock is easier to form microfracture under the action of tectonic action, and the rigid skeleton formed by quartz particles can protect the pore space from compaction damage. The higher the quartz content, the larger the pore space and the stronger the pore compaction resistance, which is helpful in maintaining the original porosity to the greatest extent [77]. Porosity is negatively correlated with clay mineral content (Figure 10d, R^2 = 0.501). This is because in the process of mineral transformation, the surface PV, interlayer PV, and aggregate PV of clay mineral particles decrease, and many diagenetic intergranular pores may be formed. Consequently, porosity loss increases as clay mineral content increases [78,79].

5.3.2. Evolution Characteristics of Pore Structure

With the increase in maturity, the micropore volume of Longtan Formation shale decreases first, reaching the minimum at Ro = 1.43%, and then gradually increasing (Figure 11a). The reason for the decrease is that the hydrocarbon generated by OM fills the original pore space, while continuous pyrolysis leads to the continuous release of

hydrocarbon gas, and the formation of many organic pores is the reason for the increase in PV. The evolution process of mesopore volume increases with the increase in maturity (Figure 11b). The overall reason may be due to the good connectivity of mesopores. When the generated liquid hydrocarbons are converted into gas, hydrocarbons are more easily released from the pores. Although the mechanical compaction effect is relatively strong, the presence of quartz particles plays a more important supporting role, thus ensuring that the PV of the mesoporous is in an increasing state as a whole.

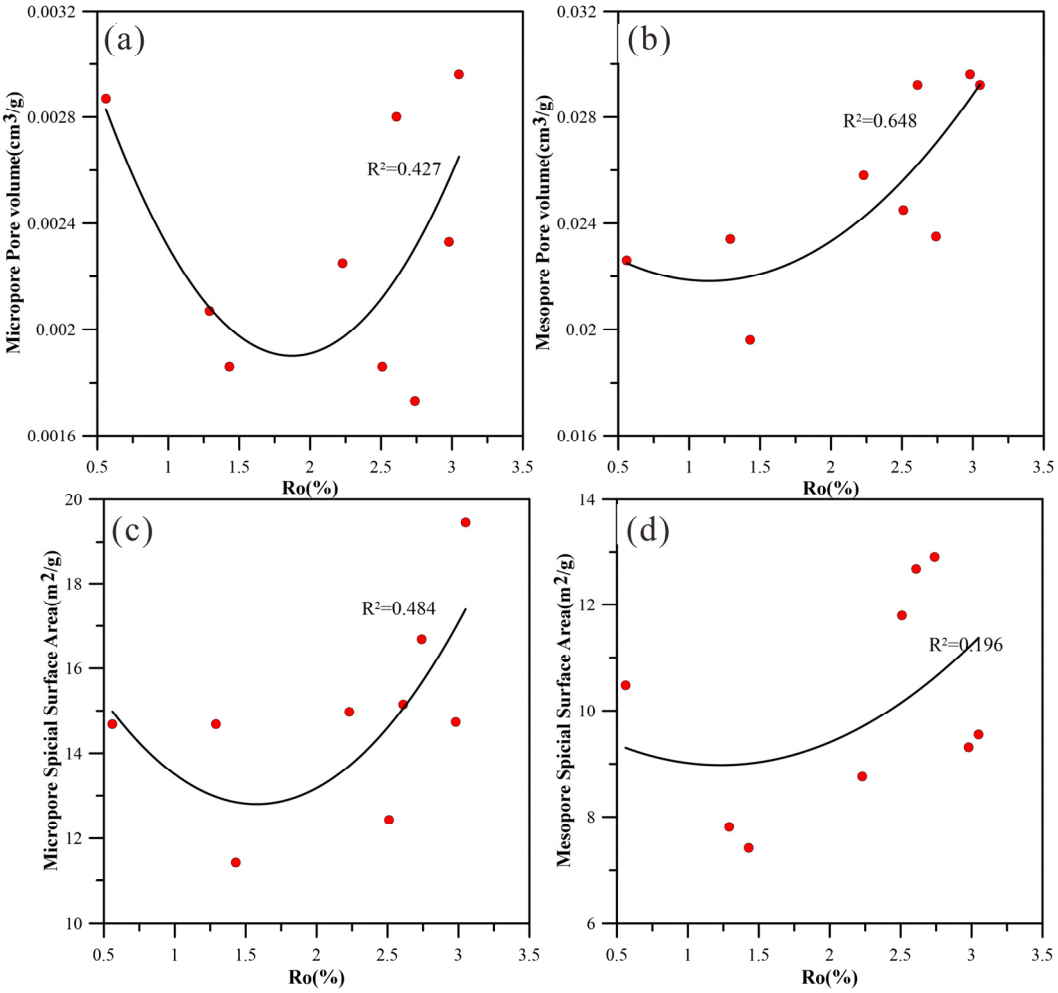

Figure 11. Evolution characteristics of PV and SSA of Longtan Formation MCFS, YJ1 well. (**a**). The Relationship between Ro and PV of Micropore; (**b**). The Relationship between Ro and PV of Mesopore; (**c**). The Relationship between Ro and SSA of Micropore; (**d**). The Relationship between Ro and SSA of Mesopore.

The SSA values of micropores and mesopores in the shale of the study area decrease first and then increase with the increase in maturity. It reaches its minimum value when the Ro ≈ 1.43% (Figure 11c,d). During the maturation process of the shale in the study area, a large amount of liquid hydrocarbons filled the pores, resulting in a decrease in SSA, and then the liquid hydrocarbons gradually converted into gas, thereby increasing the SSA of the shale micropores again. For mesopores, as the dominant mesopores, larger pores are more conducive to the circulation of liquid hydrocarbons. Therefore, the decrease in SSA is small, and on the whole, it is still in an increasing evolution state.

Due to the increase in maturity, the porosity of Longtan Formation shale reaches the minimum value at Ro = 1.43%, and then increases continuously. The volume of micropores decreases first, reaching the minimum value at Ro = 1.43%, and then increases. The volume

of mesopores is increasing. The micropore SSA first decreases, reaching a minimum at Ro = 1.43%, and then increases. The mesopores continue to increase (Figure 12).

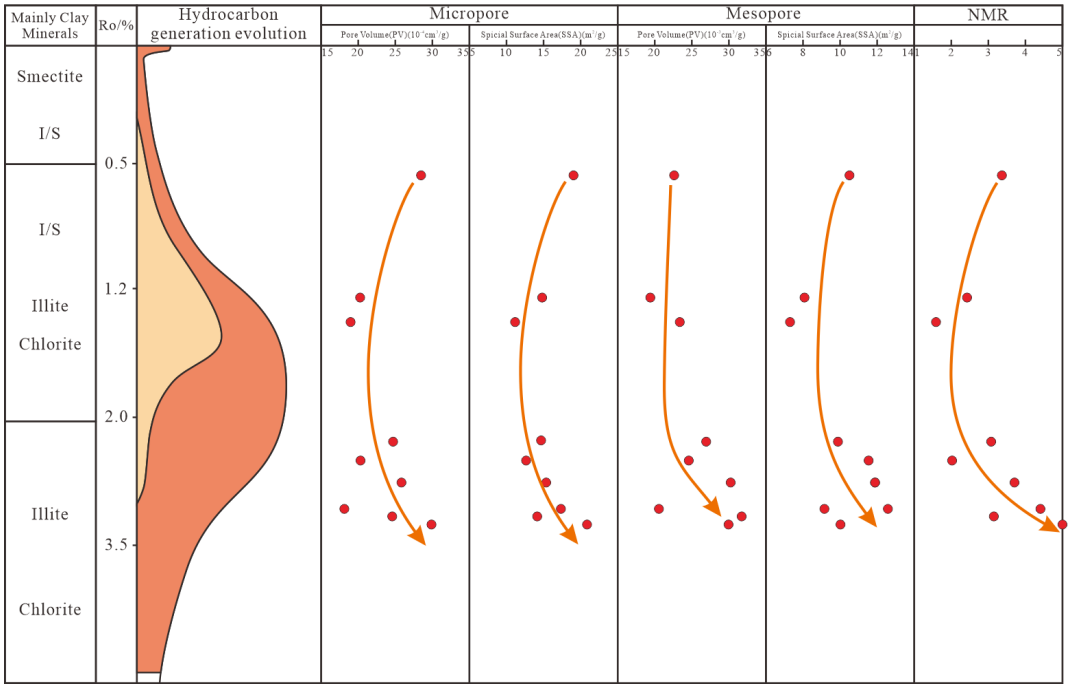

Figure 12. Pore structure evolution of Longtan Formation MCFS under diagenesis, YJ1 well.

5.4. Diagenesis-Pore Evolution Model

The evolution of pore structure in the Longtan Formation MCFS is mainly affected by two main factors: the diagenesis of minerals and the thermal evolution of OM. In different evolution stages, they have different effects on the formation and evolution of the pore system, which lead to different evolution forms (Figure 13).

1. In the immature stage (Ro < 0.5%), the Longtan Formation shale contains a significant smectite content along with a certain amount of I/S and illite. Primary pores like intragranular pores and intergranular pores dominate the pore system.
2. In the low maturity stage (0.5% < Ro < 1.3%), with the increase in maturity, OM began to enter the hydrocarbon generation stage, forming organic acids, dissolving unstable minerals (calcite and feldspar, etc.), and forming secondary matrix dissolution pores. Mixed layer I-S transforms into illite and chlorite during this phase, producing pores in dehydrated clay minerals and enlarging secondary pores [80–84].
3. After the high-over mature stage (Ro > 1.3%), plenty of OM pores are formed in the cracking gas generation stage, and the dissolution is weakened. The clay minerals in shale are mainly stable minerals such as illite and chlorite, and the pore structure of shale is almost stable.

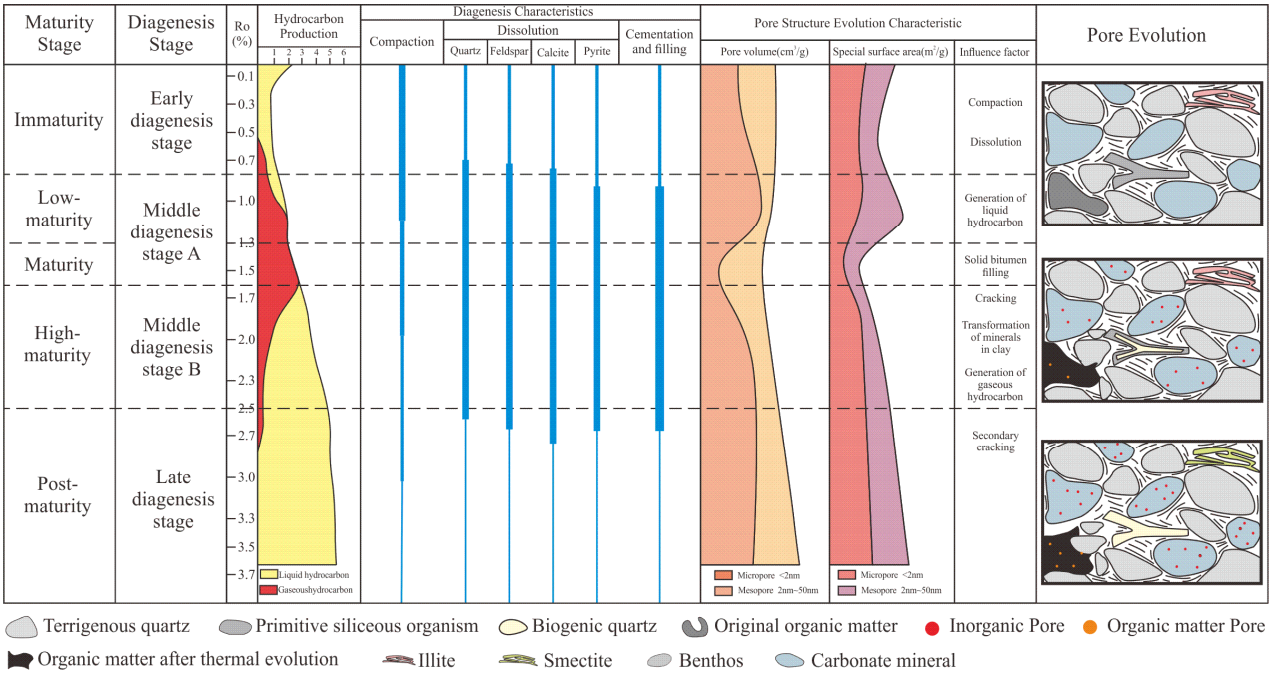

Figure 13. Diagenesis-pore evolution model of Longtan Formation MCFS, YJ1 Well (Modified according to [71]).

6. Conclusions

In this paper, XRD, FE-SEM, LPGA, and NMR were used to subdivide the diagenesis stage according to thermal maturity, clay mineral morphology, and microscopic characteristics. Combined with adsorption characteristics and image analysis, the pore structure characteristics in the process of OM evolution and hydrocarbon generation were studied. The relationship between maturity, mineral composition, PV, and SSA was discussed. The main results are as follows:

(1) The Longtan Formation shale in Southeastern Sichuan is dominated by mixed shale lithologies, and the pore system is dominated by nanoscale pores. The pore morphology of OM is different, and the pore size is small; the mineral pores are mostly irregular, and the pore size is large.

(2) The diagenetic evolution stage of the Longtan Formation MCFS enters the middle-late diagenesis stage, and each stage has corresponding evolution characteristics. In the middle diagenetic stage A, carbonate cement and clastic particles (such as feldspar) were dissolved. In the middle diagenesis stage B, smectite is widely transformed into I/S, illite, chlorite, and kaolinite. In the late diagenesis stage, the maturity varies between 0.56 and 3.05%, and the proportion of smectite in the I/S is at least 5%.

(3) When Ro < 1.43%, the porosity, PV, and SSA of micropores both decrease, while at Ro > 1.43%, the porosity, PV, and SSA of micropores increase. The PV and SSA of mesopores increased with the increase in maturity. There are two kinds of pore-reducing diagenesis: compaction and cementation, and there are two kinds of pore-increasing diagenesis: dissolution and hydrocarbon generation of OM.

(4) Maturity is an important factor controlling the evolution of pore structure. In addition, the composition of clay minerals and brittle minerals also affects the evolution of pore structure. Finally, the diagenetic evolution sequence and nano-scale pore system evolution model of Longtan Formation shale were established.

Author Contributions: Conceptualization, S.W. and B.Z.; methodology, K.M.; software, K.M. and G.C.; validation, S.W., B.Z. and K.Y.; formal analysis, P.W. and G.C.; investigation, S.W.; resources, P.W.; data curation, K.Y.; writing—original draft preparation, S.W. and B.Z.; writing—review and editing, S.W., B.Z. and C.X.; visualization, K.Y. and C.X.; supervision, B.Z.; project administration, B.Z.; funding acquisition, B.Z. All authors have read and agreed to the published version of the manuscript.

Funding: This research was funded by the National Natural Science Foundation of China (Grant No: 42272184).

Data Availability Statement: The data presented in this study are available on request from the corresponding author.

Acknowledgments: We thank the samples provided by Southwest Oil and Gas Field Branch of China National Petroleum Corporation. And I would like to thank Researcher Xu Zhengwei for his suggestions on revising the paper writing.

Conflicts of Interest: The authors declare no conflict of interest.

References

1. Nie, H.; Sun, C.; Li, P.; Jin, Z.; Liu, Q.; Bao, H.; Shen, B.; Dang, W. Carbon Isotope Evidence for Shale Gas Preservation Conditions and Large Methane Release over Million Years: A Case Study of Shale Gas Reservoirs of Wufeng and Longmaxi Formations in the Sichuan Basin. *Geosci. Front.* **2023**, *14*, 101642. [CrossRef]
2. Dong, D.; Liang, F.; Guan, Q.; Jiang, Y.; Zhou, S.; Yu, R.; Gu, Y.; Zhang, S.; Qi, L.; Liu, Y. Development Model and Identification of Evaluation Technology for Wufeng Formation–Longmaxi Formation Quality Shale Gas Reservoirs in the Sichuan Basin. *Nat. Gas Ind. B* **2023**, *10*, 165–182. [CrossRef]
3. Taghavinejad, A.; Sharifi, M.; Heidaryan, E.; Liu, K.; Ostadhassan, M. Flow Modeling in Shale Gas Reservoirs: A Comprehensive Review. *J. Nat. Gas Sci. Eng.* **2020**, *83*, 103535. [CrossRef]
4. Yang, F.; Ning, Z.; Liu, H. Fractal Characteristics of Shales from a Shale Gas Reservoir in the Sichuan Basin, China. *Fuel* **2014**, *115*, 378–384. [CrossRef]
5. MA, X.; XIE, J. The Progress and Prospects of Shale Gas Exploration and Development in Southern Sichuan Basin, SW China. *Pet. Explor. Dev. Online* **2018**, *45*, 172–182. [CrossRef]
6. Nie, H.; Li, P.; Dang, W.; Ding, J.; Sun, C.; Liu, M.; Wang, J.; Du, W.; Zhang, P.; Li, D.; et al. Enrichment Characteristics and Exploration Directions of Deep Shale Gas of Ordovician–Silurian in the Sichuan Basin and Its Surrounding Areas, China. *Pet. Explor. Dev.* **2022**, *49*, 744–757. [CrossRef]
7. Zhang, J.; Li, X.; Wei, Q.; Sun, K.; Zhang, G.; Wang, F. Characterization of Full-Sized Pore Structure and Fractal Characteristics of Marine–Continental Transitional Longtan Formation Shale of Sichuan Basin, South China. *Energy Fuels* **2017**, *31*, 10490–10504. [CrossRef]
8. Luo, Q.; Xiao, Z.; Dong, C.; Ye, X.; Li, H.; Zhang, Y.; Ma, Y.; Ma, L.; Xu, Y. The Geochemical Characteristics and Gas Potential of the Longtan Formation in the Eastern Sichuan Basin, China. *J. Pet. Sci. Eng.* **2019**, *179*, 1102–1113. [CrossRef]
9. Guo, X.; Hu, D.; Liu, R.; Wei, X.; Wei, F. Geological Conditions and Exploration Potential of Permian Marine–Continent Transitional Facies Shale Gas in the Sichuan Basin. *Nat. Gas Ind. B* **2019**, *6*, 198–204. [CrossRef]
10. Wang, X.; Mou, C.L.; Wang, Q.; Ge, X.; Chen, X.; Zhou, K.; Liang, W. Diagenesis of black shale in Longmaxi Formation, southern Sichuan Basin and its periphery. *Acta Petr. Sin.* **2015**, *36*, 1035–1047. (In Chinese with English Abstract)
11. Xie, W.; Wang, M.; Wang, H.; Ma, R.; Duan, H. Diagenesis of Shale and Its Control on Pore Structure, a Case Study from Typical Marine, Transitional and Continental Shales. *Front. Earth Sci.* **2021**, *15*, 378–394. [CrossRef]
12. Ma, K.; Zhang, B.; Wen, S.; Lin, X.; Wang, Y.; Yang, K. Quantitative Characterization and Controlling Factors of Shallow Shale Reservoir in Taiyang Anticline, Zhaotong Area, China. *Minerals* **2022**, *12*, 998. [CrossRef]
13. Zhang, B.; Wen, H.; Qing, H.; Yang, K.; Luo, Y.; Yang, H.; Wang, P.; He, L.; Xiao, W. The Influence of Depositional and Diagenetic Processes on Rock Electrical Properties: A Case Study of the Longmaxi Shale in the Sichuan Basin. *J. Pet. Sci. Eng.* **2022**, *211*, 110119. [CrossRef]
14. *SY/T 5477-2003*; The Division of Diagenetic Stages in Clastic Rocks. Petroleum Geological Exploration Professional Standardization Committee (PGEPSC): Beijing, China, 2003. (In Chinese)
15. Lin, L.; Yu, Y.; Zhai, C.; Li, Y.; Wang, Y.; Liu, G.; Guo, Y.; Gao, J. Paleogeography and shale development characteristics of the Late Permian Longtan Formation in southeastern Sichuan Basin, China. *Mari. Petro. Geo.* **2018**, *95*, 67–81. [CrossRef]
16. Xu, L.; Yang, K.; Wei, H.; Liu, L.; Jiang, Z.; Li, X.; Chen, L.; Xu, T.; Wang, X. Pore Evolution Model and Diagenetic Evolution Sequence of the Mesoproterozoic Xiamaling Shale in Zhangjiakou, Hebei. *J. Pet. Sci. Eng.* **2021**, *207*, 109115. [CrossRef]
17. Luo, J.L.; Liu, X.H.; Lin, T.; Zhang, S.; Li, B. lmpact of Diagenesis and Hydrocarbon Emplacement on Sandstone ReservoirOuality of the Yanchang Formation (Upper Triassic) in the Ordos Basin. *Acta Geo. Sin.* **2006**, *5*, 664–673. (In Chinese with English Abstract)
18. Tan, X.F.; Tian, J.C.; Li, Z.B.; Xing, X.L.; Zhang, S.P. Diagenetic character and controling factor of reservoir of Kongdian Formation of Paleogene in Dongying basin. *Coal Geo. Exp.* **2010**, *38*, 27–32. (In Chinese with English Abstract)

19. Lu, S.Q. Reservoir diagenetic seouence and its influence on pore development in the paleogene sandstones in the Dongying sag of the Bohai Bay Basin. *Petro. GeologyExper.* **2008**, *10*, 456–459+466. (In Chinese with English Abstract)
20. You, G.Q.; Pan, J.H.; Liu, S.Q.; Chen, Y.J. Diagenesis and pore evolution of Paleogenes and stone reservoir in Dongying depression. *Acta Petro. ET Mine.* **2006**, *5*, 237–242. (In Chinese with English Abstract)
21. Salman, B.; Franks, S.G. Preservation of Shallow Plagioclase Dissolution Porosity During Burial: Implications for Porosity Prediction and Aluminum Mass Balance. *AAPG Bull.* **1993**, *77*, 1488–1501.
22. Zhang, Z.H.; Hu, W.X.; Zeng, J.H.; Yu, B.S.; Lu, X.C.; Jia, H.Y. Study of Fluid-Rock Interactions in Eogene Formationin Dongying Depression, Bohai Gulf Basin. *Acta Sediment. Sin.* **2000**, *12*, 560–566. (In Chinese with English Abstract)
23. Zhang, W.C.; Li, H.; Li, H.J.; Meng, Y.L.; Yang, F.B. Genesis and distribution of secondary porosity in the deep horizon of Gaoliu area, Nanpu Sag. *Petro. Explo. Dev.* **2008**, *6*, 308–312. (In Chinese with English Abstract) [CrossRef]
24. Yuan, G.; Cao, Y.; Gluyas, J.; Li, X.; Xi, K.; Wang, Y.; Jia, Z.; Sun, P.; Oxtoby, N.H. Feldspar dissolution, authigenic clays, and quartz cements in open and closed sandstone geochemical systems during diagenesis: Typical examples from two sags in Bohai Bay Basin. *East China AAPG Bull.* **2015**, *11*, 2121–2154. [CrossRef]
25. Rahman, M.J.J.; Worden, R.H. Diagenesis and its impact on the reservoir quality of Miocene sandstones (Surma Group) from the Bengal Basin, Bangladesh. *Mar. Pet. Geol.* **2016**, *11*, 898–915. [CrossRef]
26. Guo, X.; Teng, G.; Wei, X.; Yu, L.; Lu, X.; Sun, L.; Wei, F. Occurrence mechanism and exploration potential of deep marine shale gas in Sichuan Basin. *Acta Petro. Sin.* **2022**, *43*, 453–468. (In Chinese with English Abstract)
27. Zou, C.; Dong, D.; Wang, Y.; Li, X.; Huang, J.; Wang, S.; Guan, Q.; Zhang, C.; Wang, H.; Liu, H.; et al. Shale Gas in China: Characteristics, Challenges and Prospects (II). *Pet. Explor. Dev.* **2016**, *43*, 182–196. [CrossRef]
28. Long, S.; Feng, D.; Li, F.; Du, W. Prospect Analysis of the Deep Marine Shale Gas Exploration and Development in the Sichuan Basin, China. *J. Nat. Gas Geosci.* **2018**, *3*, 181–189. [CrossRef]
29. Jiang, S.; Peng, Y.; Gao, B.; Zhang, J.; Cai, D.; Xue, G.; Bao, S.; Xu, Z.; Tang, X.; Dahdah, N. Geology and Shale Gas Resource Potentials in the Sichuan Basin, China. *Energy Explor. Exploit.* **2016**, *34*, 689–710. [CrossRef]
30. Zhang, L.; He, X.; Li, X.; Li, K.; He, J.; Zhang, Z.; Guo, J.; Chen, Y.; Liu, W. Shale Gas Exploration and Development in the Sichuan Basin: Progress, Challenge and Countermeasures. *Nat. Gas Ind. B* **2022**, *9*, 176–186. [CrossRef]
31. Zhai, G.; Wang, Y.; Zhou, Z.; Liu, G.; Yang, Y.; Li, J. "Source-Diagenesis-Accumulation" Enrichment and Accumulation Regularity of Marine Shale Gas in Southern China. *China Geol.* **2018**, *1*, 319–330. [CrossRef]
32. Xiao, H.; Jianfa, W.; Rui, Y.; Shengxian, Z.; Xiaojin, Z.; Dongjun, Z.; Deliang, Z.; Chengxu, Z. Accumulation Conditions and Key Exploration and Development Technologies of Marine Shale Gas Field in Changning-Weiyuan Block, Sichuan Basin. *Acta Pet. Sin.* **2021**, *42*, 259.
33. Wang, Y.; Zhai, G.; Liu, G.; Shi, W.; Lu, Y.; Li, J.; Zhang, Y. Geological Characteristics of Shale Gas in Different Strata of Marine Facies in South China. *J. Earth Sci.* **2021**, *32*, 725–741. [CrossRef]
34. Yang, C.; Xiong, Y.; Zhang, J.; Liu, Y.; Chen, C. Comprehensive Understanding of OM-Hosted Pores in Transitional Shale: A Case Study of Permian Longtan Shale in South China Based on Organic Petrographic Analysis, Gas Adsorption, and X-Ray Diffraction Measurements. *Energy Fuels* **2019**, *33*, 8055–8064. [CrossRef]
35. Zhang, J.; Shi, M.; Wang, D.; Tong, Z.; Hou, X.; Niu, J.; Li, X.; Li, Z.; Zhang, P.; Huang, Y. Fields and Directions for Shale Gas Exploration in China. *Nat. Gas Ind. B* **2022**, *9*, 20–32. [CrossRef]
36. Xiao, W.; Zhang, B.; Yao, Y.; Wang, Y.; Yang, H.; Yang, K. Lithofacies and sedimentary environment of shale of Permian Longtan Formation in eastern Sichuan Basin. *Lith. Reser.* **2022**, *34*, 152–162, (In Chinese with English Abstract).
37. Wen, S.; Zhang, B.; Yao, Y.; Ma, K.; Wang, Y.; Yang, K. Pyrite morphology in shale of Permian Wujiaping Formation in eastern Sichuan Basin and its indicative significance to oceanic anoxic events. *Lith. Reser.* **2023**, *35*, 1–10. (In Chinese with English Abstract)
38. Xiao, W.; Zhang, B.; Yang, K.; Wang, Y.; Wen, S.; Ma, K.; Cao, G. Geochemical Characteristics of the Upper Permian Longtan Formation from Northeastern Sichuan Basin: Implications for the Depositional Environment and Organic Matter Enrichment. *Acta Geol. Sin.* **2023**, *97*, 1196–1213. [CrossRef]
39. Yang, C.; Zhang, J.; Tang, X.; Ding, J.; Zhao, Q.; Dang, W.; Chen, H.; Su, Y.; Li, B.; Lu, D. Comparative Study on Micro-Pore Structure of Marine, Terrestrial, and Transitional Shales in Key Areas, China. *Int. J. Coal Geol.* **2017**, *171*, 76–92. [CrossRef]
40. Dong, D.; Shi, Z.; Guan, Q.; Jiang, S.; Zhang, M.; Zhang, C.; Wang, S.; Sun, S.; Yu, R.; Liu, D.; et al. Progress, challenges and prospects of shale gas exploration in the Wufeng–Longmaxi reservoirs in the Sichuan Basin. *Nat. Gas Ind.* **2018**, *38*, 67–76. (In Chinese with English Abstract) [CrossRef]
41. Cao, Q.; Ye, X.; Liu, Y.; Wang, P.; Jiang, K. Effect of Different Lithological Assemblages on Shale Reservoir Properties in the Permian Longtan Formation, Southeastern Sichuan Basin: Case Study of Well X1. *PLoS ONE* **2022**, *17*, e0271024. [CrossRef]
42. Yang, K.; Zhang, B.; Yao, Y.; Yang, H.; Zhang, H.; Xiao, W.; Wang, Y. Organic Matter Accumulation Mechanism and Characteristics in Marine-Continental Transitional Shale: A Case Study of the Upper Permian Longtan Formation from the Well F5 in Sichuan Basin, China. *J. Pet. Sci. Eng.* **2022**, *208*, 109604. [CrossRef]
43. Zhao, P.R.; Gao, B.; Guo, Z.F.; Wei, Z.H. Exploration Potential of Marine-Continental Transitional and Deep-Water Shelf Shale Gas in the Upper Permian, Sichuan Basin. *Geol. Exp.* **2020**, *42*, 335–344.
44. Chen, Y.; Shi, X.; Xu, H.; Cao, Q.; Pei, X.; Wu, W.; Wang, L.; Yang, X. Study on the Sedimentary Environments and Its Implications of Shale Reservoirs for Permian Longtan Formation in the Southeast Sichuan Basin. *Minerals* **2023**, *13*, 689. [CrossRef]

45. Yang, H.; Lin, L.; Chen, L.; Yu, Y.; Li, D.; Tian, J.; Zhou, W.; He, J. Characteristics of Mineralogy, Lithofacies of Fine-Grained Sediments and Their Relationship with Sedimentary Environment: Example from the Upper Permian Longtan Formation in the Sichuan Basin. *Energies* **2021**, *14*, 3662. [CrossRef]
46. Cao, Q.; Liu, G.; Zhang, C.; Pan, W. Sedimentary environment and its controlling on source rocks during late Permian in Sichuan Basin. Petr. *Geo. Exper.* **2013**, *35*, 36–41. (In Chinese with English Abstract)
47. He, Z.; Nie, H.; Li, S.; Liu, G.; Ding, J.; Bian, R.; Lu, Z. Differential occurence of shale gas in the Permian Longtan Formation of Upper Yangtze region constrained by plate tectonics in the Tethyan domain. *Oil Gas Geo.* **2021**, *42*, 1–15. (In Chinese with English Abstract)
48. Guo, T. Key geological issues and main controls on accumulation and enrichment of Chinese shale gas. *Petr. Expl. Dev.* **2016**, *43*, 317–326. (In Chinese with English Abstract) [CrossRef]
49. Wang, E.; Guo, T.; Liu, B.; Li, M.; Xiong, L.; Dong, X.; Zhang, N.; Wang, T. Lithofacies and Pore Features of Marine-Continental Transitional Shale and Gas Enrichment Conditions of Favorable Lithofacies: A Case Study of Permian Longtan Formation in the Lintanchang Area, Southeast of Sichuan Basin, SW China. *Pet. Explor. Dev.* **2022**, *49*, 1310–1322. [CrossRef]
50. *SY/T 5163-2010*; Analysis Method for Clay Minerals and Ordinary Ono-Clay Minerals in Sedimentary Rocks by the X-ray Diffraction. Petroleum Geological Exploration Professional Standardization Committee (PGEPSC): Beijing, China, 2010. (In Chinese)
51. He, Y.; Tang, X.; Shan, Y.; Liu, G.; Xie, H.; Ma, Z. Lithofacies division and comparison and characteristics of Longtan Formation shale in typical areas of Sichuan Basin and its surrounding. *Natu. Gas Geos.* **2021**, *32*, 174–190. (In Chinese with English Abstract)
52. Zhang, J.; Li, X.; Zhang, G.; Zou, X.; Wang, F.; Tang, Y. Microstructural Investigation of Different Nanopore Types in Marine-Continental Transitional Shales: Examples from the Longtan Formation in Southern Sichuan Basin, South China. *Mar. Pet. Geol.* **2019**, *110*, 912–927. [CrossRef]
53. Wei, Z.; Wang, Y.; Wang, G.; Sun, Z.; Xu, L. Pore Characterization of Organic-Rich Late Permian Da-Long Formation Shale in the Sichuan Basin, Southwestern China. *Fuel* **2018**, *211*, 507–516. [CrossRef]
54. Li, J.; Wang, X.; Zhou, K.; Wang, Y.; Li, N.; Wu, Y.; Wang, M. Characteristics of ultra-deep shale reservoir of marine-continental transitional facies: A case study of lower member of Upper Permian Longtan Formation in well Y4, Puguang Gas Field, northeastern Sichuan Basin. *Petr. Geo. Exper.* **2022**, *44*, 71–84. (In Chinese with English Abstract)
55. Loucks, R.G.; Reed, R.M.; Ruppel, S.C.; Hammes, U. Spectrum of Pore Types and Networks in Mudrocks and a Descriptive Classification for Matrix-Related Mudrock Pores. *AAPG Bull.* **2012**, *96*, 1071–1098. [CrossRef]
56. Thommes, M.; Kaneko, K.; Neimark, A.V.; Olivier, J.P.; Rodriguez-Reinoso, F.; Rouquerol, J.; Sing, K.S.W. Physisorption of Gases, with Special Reference to the Evaluation of Surface Area and Pore Size Distribution (IUPAC Technical Report). *Pure Appl. Chem.* **2015**, *87*, 1051–1069. [CrossRef]
57. Kfeinberg, R.L.; Straley, C.; Kenyon, W.E.; Akkurt, R.; Farooqui, S.A. *Nuclear Magnetic Resonance of Rocks: T1 vs. T2*; OnePetro: Richardson, TX, USA, 1993.
58. Yao, Y.; Liu, J.; Liu, D.; Chen, J.; Pan, Z. A New Application of NMR in Characterization of Multiphase Methane and Adsorption Capacity of Shale. *Int. J. Coal Geol.* **2019**, *201*, 76–85. [CrossRef]
59. Sun, J.; Chen, J.; Yang, Z.; Liu, X.; Liu, Y. Experimental Study of the NMR Characteristics of Shale Reservoir Rock. *Sci. Tech. Rev.* **2012**, *30*, 25–30. (In Chinese with English Abstract)
60. Tan, M.; Mao, K.; Song, X.; Yang, X.; Xu, J. NMR Petrophysical Interpretation Method of Gas Shale Based on Core NMR Experiment. *J. Pet. Sci. Eng.* **2015**, *136*, 100–111. [CrossRef]
61. Xu, H.; Tang, D.; Zhao, J.; Li, S. A Precise Measurement Method for Shale Porosity with Low-Field Nuclear Magnetic Resonance: A Case Study of the Carboniferous–Permian Strata in the Linxing Area, Eastern Ordos Basin, China. *Fuel* **2015**, *143*, 47–54. [CrossRef]
62. Huang, J.; Xu, K.; Guo, S.; Guo, H. Comprehensive Study on Pore Structures of Shale Reservoirs Based on SEM, NMR and X-CT. *Geoscience* **2015**, *29*, 198–205. (In Chinese with English Abstract)
63. Zhao, W.; Yang, L.; Jiang, Z.; He, W.; Huang, L.; Chang, Q.; Tang, X.; Ye, H. Geneses of Multi-Stage Carbonate Minerals and Their Control on Reservoir Physical Properties of Dolomitic Shales. *Mar. Pet. Geol.* **2023**, *153*, 106216. [CrossRef]
64. Zhao, K.; Du, X.; Lu, Y.; Hao, F.; Liu, Z.; Jia, J. Is volcanic ash responsible for the enrichment of organic carbon in shales? Quantitative characterization of organic-rich shale at the Ordovician-Silurian transition. *Bulletin* **2021**, *133*, 837–848. [CrossRef]
65. Zhou, X.; Li, X.; Guo, W.; Zhang, X.; Liang, P.; Yu, J. Characteristics, Formation Mechanism and Influence on Physical Properties of Carbonate Minerals in Shale Reservoirs of Wufeng-Longmaxi Formations, Sichuan Basin, China. *J. Nat. Gas Geosci.* **2022**, *7*, 133–146. [CrossRef]
66. Aldega, L.; Carminati, E.; Scharf, A.; Mattern, F. Thermal maturity of the Hawasina units and origin of the Batinah Mélange (Oman Mountains): Insights from clay minerals. *Mar. Petro. Geo.* **2021**, *133*, 105316. [CrossRef]
67. Aldega, L.; Corrado, S.; Dipaolo, L.; Somma, R.; Maniscalco, R.; Balestrieri, M.L. Shallow burial and exhumation of the Peloritani Mts. (NE Sicily, Italy): Insight from paleo-thermal and structural indicators. *Geo. Soci. of Ame. Bull.* **2011**, *123*, 132–149. [CrossRef]
68. Wang, G.; Jin, Z.; Zhang, Q.; Zhu, R.; Tang, X.; Liu, K.; Dong, L. Effects of Clay Minerals and Organic Matter on Pore Evolution of the Early Mature Lacustrine Shale in the Ordos Basin, China. *J. Asian Earth Sci.* **2023**, *246*, 105516. [CrossRef]
69. Li, J.; Ma, Y.; Huang, K.; Zhang, Y.; Wang, W.; Liu, J.; Li, Z.; Lu, S. Quantitative Characterization of Organic Acid Generation, Decarboxylation, and Dissolution in a Shale Reservoir and the Corresponding Applications—A Case Study of the Bohai Bay Basin. *Fuel* **2018**, *214*, 538–545. [CrossRef]

70. Su, A.; Chen, H.; Feng, Y.; Zhao, J.; Nguyen, A.D. Multistage Fracturing History in the Paleocene Lacustrine Shale Oil Reservoirs of the Subei Basin, Eastern China. *Mar. Pet. Geol.* **2022**, *144*, 105835. [CrossRef]
71. Ma, X.; Guo, S. Study on Pore Evolution and Diagenesis Division of a Permian Longtan Transitional Shale in Southwest Guizhou, China. *Energy Sci. Eng.* **2021**, *9*, 58–79. [CrossRef]
72. Galushkin, Y.I. Thermal effects of igneous intrusions on maturity of organic matter: A possible mechanism of intrusion. *Org. Geochem.* **1997**, *5*, 645–658. [CrossRef]
73. Olsson, I. Regional burial heating vs. *local magmatic heat influence of the Röstånga area, Scania, southern Sweden GFF* **1999**, *121*, 209–214.
74. Stagpoole, V.; Funnell, R. Arc magmatism and hydrocarbon generation in the northern Taranaki Basin, New Zealand. *Pet. Geosci.* **2001**, *7*, 255–267.
75. Wang, R.; Hu, Z.; Bao, H.; Wu, J.; Du, W.; Wang, P.; Peng, Z.; Lu, T. Diagenetic evolution of key minerals and its controls on reservoir quality of Upper Ordovician Wufeng-Lower Silurian Longmaxi shale of Sichuan Basin. *Petr. Geo. Exper.* **2021**, *43*, 996–1005. (In Chinese with English Abstract)
76. Chen, X.; Qu, X.; Xu, S.; Wang, W.; Li, S.; He, H.; Liu, Y. Dissolution Pores in Shale and Their Influence on Reservoir Quality in Damintun Depression, Bohai Bay Basin, East China: Insights from SEM Images, N2 Adsorption and Fluid-Rock Interaction Experiments. *Mar. Pet. Geol.* **2020**, *117*, 104394. [CrossRef]
77. Ismail, I.M.K.; Pfeifer, P. Fractal Analysis and Surface Roughness of Nonporous Carbon Fibers and Carbon Blacks. *Langmuir* **1994**, *10*, 1532–1538. [CrossRef]
78. Ross, D.J.K.; Marc Bustin, R. The Importance of Shale Composition and Pore Structure upon Gas Storage Potential of Shale Gas Reservoirs. *Mar. Pet. Geol.* **2009**, *26*, 916–927. [CrossRef]
79. Ma, Y.; Zhong, N.; Li, D.; Pan, Z.; Cheng, L.; Liu, K. Organic Matter/Clay Mineral Intergranular Pores in the Lower Cambrian Lujiaping Shale in the North-Eastern Part of the Upper Yangtze Area, China: A Possible Microscopic Mechanism for Gas Preservation. *Int. J. Coal Geol.* **2015**, *137*, 38–54. [CrossRef]
80. Liu, B.; Bai, L.; Chi, Y.; Jia, R.; Fu, X.; Yang, L. Geochemical Characterization and Quantitative Evaluation of Shale Oil Reservoir by Two-Dimensional Nuclear Magnetic Resonance and Quantitative Grain Fluorescence on Extract: A Case Study from the Qingshankou Formation in Southern Songliao Basin, Northeast China. *Mar. Pet. Geol.* **2019**, *109*, 561–573.
81. Guo, X.; Qin, Z.; Yang, R.; Dong, T.; He, S.; Hao, F.; Yi, J.; Shu, Z.; Bao, H.; Liu, K. Comparison of Pore Systems of Clay-Rich and Silica-Rich Gas Shales in the Lower Silurian Longmaxi Formation from the Jiaoshiba Area in the Eastern Sichuan Basin, China. *Mar. Pet. Geol.* **2019**, *101*, 265–280. [CrossRef]
82. Liu, D.; Li, Z.; Jiang, Z.; Zhang, C.; Zhang, Z.; Wang, J.; Yang, D.; Song, Y.; Luo, Q. Impact of Laminae on Pore Structures of Lacustrine Shales in the Southern Songliao Basin, NE China. *J. Asian Earth Sci.* **2019**, *182*, 103935. [CrossRef]
83. Xu, H.; Zhou, W.; Hu, Q.; Yi, T.; Ke, J.; Zhao, A.; Lei, Z.; Yu, Y. Quartz Types, Silica Sources and Their Implications for Porosity Evolution and Rock Mechanics in the Paleozoic Longmaxi Formation Shale, Sichuan Basin. *Mar. Pet. Geol.* **2021**, *128*, 105036. [CrossRef]
84. Xu, J.; Wu, S.; Liu, J.; Yuan, Y.; Cui, J.; Su, L.; Jiang, X.; Wang, J. New Insights into Controlling Factors of Pore Evolution in Organic-Rich Shale. *Energy Fuels* **2021**, *35*, 4858–4873. [CrossRef]